Theoretical and experimental determination of L-shell decay rates, line widths, and fluorescence yields in Ge

M. Guerra,[1,*] J. M. Sampaio,[2] T. I. Madeira,[2] F. Parente,[1] P. Indelicato,[3] J. P. Marques,[2] J. P. Santos,[1,†] J. Hoszowska,[4] J.-Cl. Dousse,[4] L. Loperetti,[4] F. Zeeshan,[4] M. Müller,[5] R. Unterumsberger,[5] and B. Beckhoff[5]

[1]*Laboratório de Instrumentação, Engenharia Biomédica e Física da Radiação (LIBPhys-UNL), Departamento de Física, Faculdade de Ciências e Tecnologia, FCT, Universidade Nova de Lisboa, 2829-516 Caparica, Portugal*

[2]*BioISI—Biosystems & Integrative Sciences Institute, Faculdade de Ciências da Universidade de Lisboa, Campo Grande C8, 1749-016 Lisboa, Portugal*

[3]*Laboratoire Kastler Brossel, École Normale Supérieure, CNRS, Sorbonne Universités, UPMC Université Paris 06, Case 74, 4 place Jussieu, 75005 Paris, France*

[4]*Physics Department, University of Fribourg, Chemin du Musée 3, CH-1700 Fribourg, Switzerland*

[5]*Physikalisch-Technische Bundesanstalt (PTB), Abbestraße 2-12, 10587 Berlin, Germany*

(Received 14 May 2015; published 19 August 2015)

Fluorescence yields (FYs) for the Ge L shell were determined by a theoretical and two experimental groups within the framework of the International Initiative on X-Ray Fundamental Parameters Collaboration. Calculations were performed using the Dirac-Fock method, including relativistic and QED corrections. The experimental value of the L_3 FY ω_{L_3} was determined at the Physikalisch-Technische Bundesanstalt undulator beamline of the synchrotron radiation facility BESSY II in Berlin, Germany, and the $L\alpha_{1,2}$ and $L\beta_1$ line widths were measured at the Swiss Light Source, Paul Scherrer Institute, Switzerland, using monochromatized synchrotron radiation and a von Hamos x-ray crystal spectrometer. The measured fluorescence yields and line widths are compared to the corresponding calculated values.

DOI: 10.1103/PhysRevA.92.022507 PACS number(s): 31.30.jf, 32.70.Jz, 32.30.Rj

I. INTRODUCTION

When a hole is created in one of the L subshells of an atom or ion by a photon or particle collision, the target's electronic structure can suffer a rearrangement through the shifting of electrons from one subshell to another. This process may lead to the emission of an x-ray photon (radiative transition) or to the emission of an electron from an outer shell, carrying the excess energy (radiationless transition, also called Auger emission). In particular, if, in the latter case, the vacancy is filled by an electron from a higher subshell of the same shell, we call it a Coster-Kronig (CK) transition [1] or, if, in addition, the emitted electron also belongs to the same shell, a super-CK transition.

L-shell radiative transitions are labeled, according to the Siegbahn notation, $L\alpha$, $L\beta$, and $L\gamma$ transitions, depending on the final-hole shell. In Fig. 1, the transitions that give rise to the L lines are presented schematically and the correspondence among the Siegbahn, IUPAC, and *nlj* electron configuration (EC) notations is also shown [2,3]. Following the same reasoning, radiationless transitions are described by identifying the subshells where the initial and final holes lie. For example, the process that involves a transition of the initial hole in the L_1 subshell to the L_3 subshell, with the ejection of an M_4 electron, is identified as the L_1-L_3M_4 transition.

The knowledge of accurate values of decay rates, for both radiative and radiationless transitions, is of paramount importance for understanding collision dynamics and photon-atom or particle-atom interactions, as well as in several applied fields such as x-ray fluorescence, proton-induced x-ray emission, Auger electron spectroscopy, electron energy loss spectroscopy, and electron probe microanalysis. One of the most important parameters is the fluorescence yield (FY), defined as the relative probability that a hole in a given shell or subshell is filled through a radiative transition. FYs are needed in many areas related to physics, namely, in quantitative elemental analysis of samples in x-ray spectroscopy to derive the energy-absorption coefficients related to dosimetric quantities, in plasma physics, to characterize the emitted x-ray spectra, and in astrophysics to compute the emission and absorption lines in stellar objects.

In the 1960s and early 1970s, several groups were engaged in the determination of x-ray FYs and decay rates both theoretically and experimentally. The theoretical calculations, however, were essentially nonrelativistic [4–7] except for Bhalla's calculation of M-shell radiative transition probabilities, which used the Dirac-Hartree-Slater approach [8]. In the early 1980s, Chen *et al.* performed a series of relativistic calculations of K [9]-, L [10]-, and M [11,12]-shell radiationless transitions for several elements from $Z = 18$ to $Z = 96$, also based on the Dirac-Hartree-Slater approach. They showed that relativistic values in individual transitions are enhanced by between 10% and 50% relative to nonrelativistic values. These results also pointed out the importance of going beyond an independent particle model towards a multiconfiguration calculation.

Recently, the multiconfiguration Dirac-Fock method has been employed in the calculation of decay rates, widths, and FYs, for the K shell of Ge [13], for the M shell of Zn, Cd, and Hg [14], and for the $K\alpha_{1,2}$ line width of Al and Si [15].

In the last decade there was an increase in high-precision measurements of FYs [13,16–19] but only for the K shell, while results for the L shell are very scarce and results for the M shell are almost nonexistent.

In this work, we present the results of a collaboration between experimental and theoretical groups to obtain very

*mguerra@fct.unl.pt

†jps@fct.unl.pt

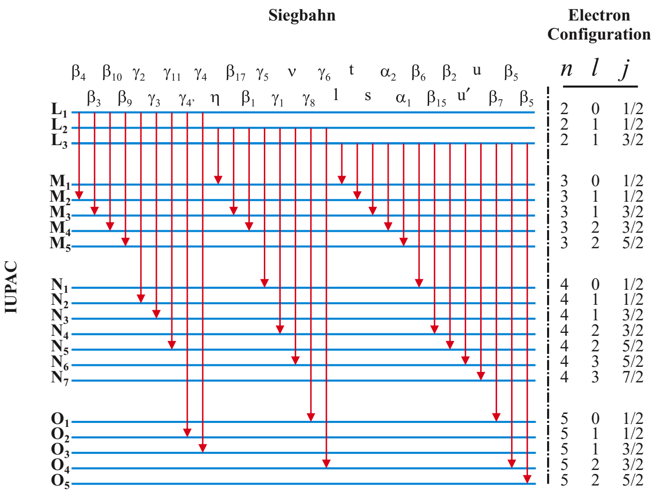

FIG. 1. (Color online) Correspondence among the Siegbahn, IUPAC, and nlj electron configuration notations for radiative transitions [3], where n is the principal quantum number, l is the orbital angular momentum, and j is the total angular momentum quantum number.

precise results for L-shell decay rates, line widths, and FYs in Ge. The article is organized as follows: a brief explanation of the principles employed in the multiconfiguration Dirac-Fock calculations of decay rates and FYs is given in Sec. II, and the experimental methodologies are described in Sec. III. Experimental and theoretical results are presented and discussed in Sec. IV. Comparisons with previous data are made in Sec. V, and conclusions drawn from the obtained results.

II. THEORY

All wave functions and matrix elements obtained in this work were calculated with the relativistic general purpose multiconfiguration Dirac-Fock code (MCDFGME) developed by Desclaux and Indelicato [20,21].

A. Relativistic calculations

L-shell radiative and radiationless decay rates for Ge were calculated using the code in the single-configuration approach, with the Breit interaction and the vacuum polarization terms included in the self-consistent field calculation, and other QED effects, such as self-energy and vacuum polarization, included as perturbations [22–25]. A detailed description of the Hamiltonian and wave functions is given in Refs. [22,26–28]. The so-called optimized levels (OLs) method was used to calculate the wave functions and energies of the levels involved in all possible transitions, considering full relaxation of both initial and final states, hence providing more accurate energies and wave functions. Since the spin orbitals of the initial and final levels were optimized separately, they are not orthogonal. To deal with the nonorthogonality of the wave functions, the code uses the formalism described by Löwdin [29].

Regarding the radiationless transitions, we have assumed a two-step process, in which the decay is independent of the ionization. Hence, the electron ejected in the process of creation of the initial hole does not interact with the Auger electron, and the core-hole state interacts very weakly with the latter electron, allowing for the transition rates to be calculated from perturbation theory. Initial-state wave functions were generated for configurations that contain one initial inner-shell vacancy, while final-state wave functions were generated for configurations that contain two higher shell vacancies. Continuum-state wave functions were obtained by solving the Dirac-Fock equations with the same atomic potential of the initial state, normalized to represent one ejected electron per unit energy.

In order to keep consistency between the radiative and the radiationless calculations, multiconfiguration wave functions beyond intermediate coupling were not employed, because the approximation used for the evaluation of the Auger rate cannot be used in an optimized level calculation with correlation orbitals.

B. Decay rates, subshell widths, and fluorescence yields

The width of an atomic level i is given by $\Gamma_i = \hbar \sum_j W_{ij}$, where W_{ij} is the transition probability from level i to all possible final levels j, including contributions from radiative and radiationless processes, and is given by the sum of the radiative Γ_{R}, Auger Γ_{A}, and CK Γ_{CK}, widths.

If the system has no unpaired outer electrons, or if the interaction between the hole and those electrons is neglected, only one level corresponds to each one-hole configuration. Therefore the width of the configuration is just the width of the corresponding level.

The situation is more complicated, in general, if the interaction with existing unpaired electrons is taken into account. The fine structure resulting from the interaction between the inner hole and these electrons leads to a number of different levels for a given configuration, each one identified by a particular value of the total angular momentum J and by the electronic coupling. This is the case for Ge, where two p electrons exist in the outermost shell.

Assuming that the initial one-hole S_n-subshell multiplet levels, identified by the total angular momentum J_i and the coupling scheme, are statistically populated (in the experiments carried out in this work there is no preferential population of any given magnetic sublevel), the radiative (R) width of a subshell S_n is obtained by summing the partial widths, $\Gamma^{\mathrm{R}}_{i,j}$, for all levels i of the system with one hole in subshell S_n decaying radiatively to all levels j of the system with one hole in a higher subshell:

$$\Gamma^{\mathrm{R}}_{S_n} = \frac{\sum_i \sum_j (2J_i+1)\Gamma^{\mathrm{R}}_{i,j}}{\sum_i (2J_i+1)}. \tag{1}$$

Here,

$$\Gamma^{\mathrm{R}}_{i,j} = \hbar W^{\mathrm{R}}_{i,j}. \tag{2}$$

In the same way, the radiationless width of the subshell S_n is given by

$$\Gamma^{\mathrm{NR}}_{S_n} = \frac{\sum_i \sum_j (2J_i+1)\Gamma^{\mathrm{NR}}_{i,k}}{\sum_i (2J_i+1)}, \tag{3}$$

TABLE I. Calculated width (in eV) of the L_1, L_2, L_3, M_1, M_2, M_3, M_4, and M_5 one-hole configurations.

	L_1	L_2	L_3	M_1	M_2	M_3	M_4	M_5
This work (theoretical)	6.11	0.94	0.98	2.19	3.26	2.98	0.013	0.012
EADL [31]	8.71	0.84	0.84	4.13	3.99	3.71	0.05	0.044
Campbell [30]	3.8	0.86	0.86	2.1	2.3	2.3	0.05	0.044

where

$$\Gamma_{i,k}^{\mathrm{NR}} = \hbar W_{i,k}^{\mathrm{NR}}. \tag{4}$$

Here $W_{i,k}^{\mathrm{NR}}$ is the radiationless transition probability from level i to level k. Thus, $\Gamma_{i,k}^{\mathrm{NR}}$ is the partial width corresponding to the radiationless transition from level i in the system with one hole in susbshell S_n to level k of the system with two holes in higher shells or subshells, with the emission of an electron to the continuum.

Henceforth, the index i is related to the configuration S_n and spans over all possible initial levels (with different total angular momenta, J_i). The final levels of the system, with one or two holes, corresponding to radiative and radiationless transitions, respectively, are denoted by the indices j and k.

Radiationless widths include contributions from Auger, CK, and super-CK transitions. In the Auger contributions, the original hole is filled by an electron from a higher shell and a second electron is emitted also from a higher shell; in the CK contributions, the initial hole is filled by an electron from the same shell and the emitted electron belongs to a higher shell or to another subshell of the same shell. The latter are also called super-CK transitions. Thus, the (total) width of an S_n shell is

$$\Gamma_{S_n} = \Gamma_{S_n}^{\mathrm{R}} + \Gamma_{S_n}^{\mathrm{NR}}. \tag{5}$$

The widths of the Ge L and M subshells computed in this work using this equation are listed in Table I together with the recommended values of Campbell and Papp [30] and the EADL values [31].

The FY of an atomic subshell is defined as the probability that the vacancy in that subshell is filled through a radiative transition and, if we neglect other less probable modes of decay, such as two photon transitions, hyperfine quenchings, etc., is given by

$$\omega_{S_n} = \frac{\Gamma_{S_n}^{\mathrm{R}}}{\Gamma_{S_n}^{\mathrm{R}} + \Gamma_{S_n}^{\mathrm{NR}}}, \tag{6}$$

where for the L shell, the indices $n = 1$, 2, and 3 denote holes in the orbitals $2s_{1/2}$, $2p_{1/2}$, and $2p_{3/2}$, respectively.

Assuming that the initial L-subshell multiplet levels, identified by the total angular momentum J_i, are statistically populated, and considering the relation between the natural widths and the decay rates, Eq. (6) may be written as

$$\omega_{L_n} = \frac{\sum_i \sum_j (2J_i+1) W_{i,j}^{\mathrm{R}}}{\sum_i (2J_i+1)\left(\sum_j W_{i,j}^{\mathrm{R}} + \sum_k W_{i,k}^{\mathrm{NR}}\right)}, \tag{7}$$

where $W_{i,j}^{\mathrm{R}}$ and $W_{i,k}^{\mathrm{NR}}$ stand for the radiative and radiationless decay rates, respectively, of the initial one-hole level i in the L_n subshell to a one-hole level j or to a two-hole level k. Similarly to the FY, the Auger a_{L_n} yield for the L subshells is defined as

$$a_{L_n} = \frac{\sum_{i,k} (2J_i+1)\left(W_{i,k}^{\mathrm{NR}}\right)}{\sum_i (2J_i+1)\left(\sum_j W_{i,j}^{\mathrm{R}} + \sum_k W_{i,k}^{\mathrm{NR}}\right)}, \tag{8}$$

where the k index refers to levels with two holes in M, N, or higher shells. On the other hand, the CK $f_{L_n,L_{n'}}$ yields for the L subshells are given by an identical expression,

$$f_{L_n,L_{n'}} = \frac{\sum_{i,k'} (2J_i+1)\left(W_{i,k'}^{\mathrm{NR}}\right)}{\sum_i (2J_i+1)\left(\sum_j W_{i,j}^{\mathrm{R}} + \sum_{k'} W_{i,k'}^{\mathrm{NR}}\right)}, \tag{9}$$

but in this equation the k' index refers to levels with one hole in a subshell L'_n ($n < n'$) and a second hole in a higher shell.

From these definitions, one can conclude that the following relation is valid for each subshell L_n:

$$\omega_{L_n} + a_{L_n} + \sum_{n'>n} f_{L_n,L_{n'}} = 1. \tag{10}$$

C. Line widths

The theoretical width of a line corresponding to the radiative transition between two atomic levels is the sum of the widths of the two levels involved. As referred to above, when no unpaired outer electrons exist, or the interaction between the hole and those electrons is neglected, just one level corresponds to each one-hole configuration. In these cases the width of the one line corresponding to the transition between two one-hole configurations is just the sum of the widths of the initial and final levels. However, in most cases, unpaired outer electrons exist and a given number of levels correspond to the initial and final configurations, leading to a set of individual component lines. This is the case for Ge, where two unpaired $4p$ electrons exist. Nevertheless, we calculated the $L\alpha_1$, $L\alpha_2$, and $L\beta_1$ line widths by adding the widths of the L_3 and M_5, L_3 and M_4, and L_2 and M_4 subshells, respectively. The results are listed in Table II.

The component lines referred to above are usually spread out in energy, leading to an enlargement of the observable

TABLE II. Measured and calculated widths of the L_{α_1}, L_{α_2}, $L_{\alpha_{1,2}}$, and L_{β_1} lines (in eV). The notation 0.933(62/17) means (0.933 ± 0.062) eV with an included statistical uncertainty of 0.017 eV. Experimental $L\alpha_{1,2}$ widths were obtained from fits with a single Lorentzian function of the experimental data. Theoretical widths of the L_{α_1} and L_{α_2} lines were calculated by summing the initial and final subshell widths, while the $L\alpha_{1,2}$ width corresponds to the FWHM of the $L\alpha_{1,2}$ synthesized spectrum (Fig. 3) minus the experimental broadening.

	SR beam energy (keV)	L_{α_1}	L_{α_2}	$L_{\alpha_{1,2}}$	L_{β_1}
This work (theoretical)		0.992	0.993	0.928	0.954
EADL [31]		0.884	0.890		0.890
Campbell [30]		0.904	0.910		0.905
This work (experimental)	1.23			0.811(60/8)	–
	1.30			0.875(60/8)	0.933(62/17)
	1.45			0.859(60/6)	0.955(62/24)

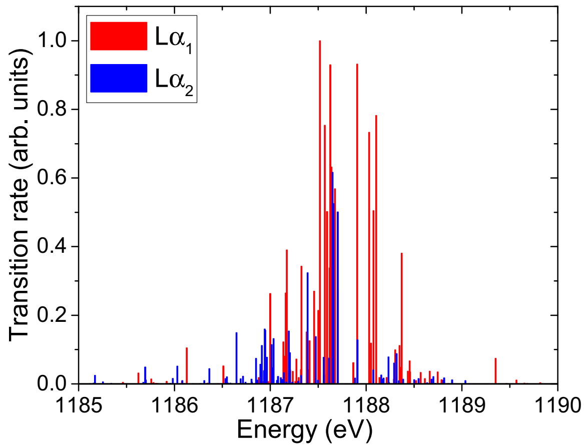

FIG. 2. (Color online) Normalized calculated transition rates in the Ge $L\alpha_{1,2}$-line manifold.

width. One remarkable example is the width of the $K\alpha_{1,2}$ line for low- and medium-Z atoms [15], whose comparison to experimental values has to be performed very carefully for this exact reason.

In Ge, the $L\alpha_{1,2}$-line manifold is made up of a set of a large number of lines corresponding to transitions between initial and final fine-structure atomic levels belonging, respectively, to a configuration with one hole in the L_3 subshell and configurations with one hole in the M_4 and M_5 subshells, respectively. The two sets of lines are spread in energy and superimposed, making a clear separation of the $L\alpha_1$ and $L\alpha_2$ "lines" impossible, as shown in Fig. 2. We obtained the width of all individual levels in the initial and final one-hole configurations by calculating the radiative and radiationless transition probabilities from each of those levels to all possible final levels. In order to compare the theoretical results to the experimental spectrum, one has to include the experimental resolution on the synthesized spectrum. This, however, is not straightforward, since the experimental broadening is obtained

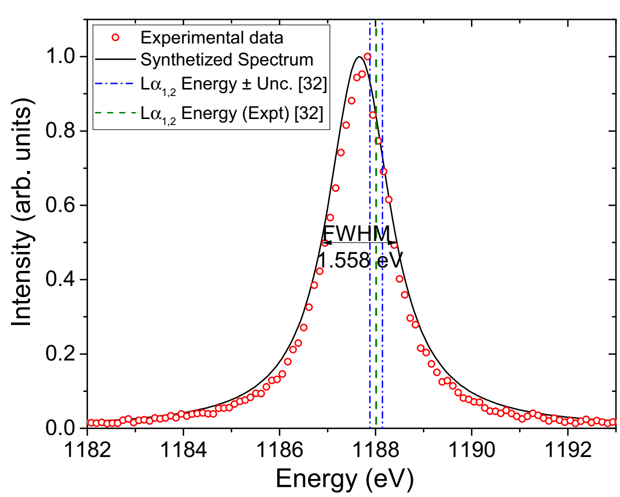

FIG. 3. (Color online) Ge $L\alpha_{1,2}$ synthesized spectrum compared to experimental data at a beam energy of 1.23 keV. The combined $L\alpha_{1,2}$ experimental energy values of Deslattes *et al.* [32] are also shown.

from a one- or two-component fit to the Mg K_{α_1} and Se L_{α_1} lines (see Sec. III), whereas for the Se $L_{\alpha_{1,2}}$ we find the same overlap between the two lines as in Ge. Thus, the inclusion of the experimental broadening in the synthesized spectrum can be performed correctly only if one assumes a two-component line for the Ge $L_{\alpha_{1,2}}$ manifold. With this in mind we have calculated the energy centroid of the L_{α_1} and L_{α_2} lines through a line intensity weighted average of the individual level energies. Due to the Lorentzian profile of the experimental broadening, we have adopted a Lorentzian distribution for each of the two resulting lines, whose width is given by our theoretical results in Table II plus the experimental broadening of 0.63 eV. The obtained normalized profile is shown together with the experimental values, at a beam energy of 1.23 keV, in Fig. 3.

III. EXPERIMENT

A. Fluorescence yields

The FY of the Ge L_3 subshell has been determined by means of reference-free x-ray fluorescence spectrometry [19] using very thin freestanding foils as specimens with a well-known composition. This approach is described in several recent publications [16,33–35] and we provide only a brief description here. A freestanding Ge foil with a nominal thickness of 300 nm and a purity of 99.99% was used for the experiments, which were carried out at the Physikalisch-Technische Bundesanstalt (PTB) plane grating monochromator beamline for undulator radiation at the synchrotron radiation facility BESSY II [36]. The Ge foil was irradiated with a monochromatic x-ray beam under an angle of incidence γ_1 of 45°. Three photon energies E_0 between the Ge L_3- and L_2-subshell absorption edges (1220, 1225, and 1231 eV) were used to excite the specimen and the incident photon flux I_0 was recorded with a radiometrically calibrated photodiode [37]. An energy-dispersive silicon-drift detector, which was calibrated with respect to both the detection efficiency $\epsilon_{\text{set}}(E_{X_i})$ and the response behavior [38], was positioned at an observation angle γ_2 of 45°. In front of the silicon-drift detector a calibrated diaphragm was placed at a well-known distance in order to define accurately the solid angle $d\Omega$ of detection. Using this detector, the fluorescence radiation emitted by the Ge foil in the solid angle defined by the diaphragm was measured. In addition, transmission measurements in a wide energy range below and above the L_3 absorption edge, including the three selected excitation energies as well as at the two fluorescence line energies of interest, have been performed. From the transmission I_{tr}/I_0 of the Ge foil the product of the Ge mass absorption cross section μ_E, the density ρ, and the thickness d of the foil could be derived directly without using any database values for the absorption cross sections. The detected count rate N_i of the fluorescence radiation of line i (L_α or L_l) having photon energy E_i is

$$N_i = I_0 \frac{d\Omega}{4\pi} \epsilon_{\text{det}}(E_i) M_i(E_0) \frac{\rho d}{\sin(\gamma_1)} \tau_{E_0} \omega_{L_3} g_i, \tag{11}$$

where

$$M_i(E_0) = \frac{1}{\rho d \mu_{E_0}/\sin(\gamma_1) + \rho d \mu_{E_i}/\sin(\gamma_2)} \times \left(1 - e^{\rho d \mu_{E_0}/\sin(\gamma_1) + \rho d \mu_{E_i}/\sin(\gamma_2)}\right) \tag{12}$$

is the absorption correction factor derived from transmission measurements, and ω_{L_3} is the FY of the L_3 subshell to be determined, g_i is the probability of emission of line i (L_α or L_l), and τ_{E_0} is the photoelectric cross section for Ge.

Using the fact that the scattering cross sections of Ge for the low photon energies involved here are only about 0.1% of the mass absorption cross section μ_{E_0}, the photoelectric cross section τ_{E_0} can be approximated very well by the L_3 contribution of μ_{E_0}. The L_3 contribution of μ_{E_0} can be obtained by extrapolating the higher shell photoelectric cross section contributions $\mu_{M,N}$, the energy dependence of which can be derived below the L_3 edge, to the excitation energies above the L_3 edge. Using the transmission measurements, the term $\rho d/\sin(\gamma_1)\tau_{E_0}$ can be substituted by $[\log(I_{tr}/I_0) - u_{M,N,E_0}]$ [16].

The transition probability g_i for both the L_α and the L_l lines can be derived from the detected count rates of both lines when corrected for both the detector efficiency and the absorption effects. Values of 0.950 ± 0.002 and 0.050 ± 0.002 were determined for g_{L_α} and g_{L_l}, respectively. At this point all parameters in Eq. (11) except the FY ω_{L_3} are known from the instrumental calibration and experimental determinations. The FY of the Ge L_3 subshell can now be derived without using any parameters from databases with frequently unknown uncertainties. We derived a value of $(1.20 \pm 0.11) \times 10^{-2}$ for the FY of the Ge L_3 subshell. The standard deviation of the FY derived at three excitation energies between L_3 and L_2 is 0.04×10^{-2} and originates mainly from the uncertainty of the spectral deconvolution, which was used to derive the detected count rates of the fluorescence lines. The other main contributions to the total relative uncertainty of 9.2% are caused by the determination of the absorption correction factor (5%) and the extrapolation of M- and N-shell contributions to μ_{E_0} (about 21%) above the L_3 absorption edge (6%). Future works at PTB will aim at the completion of subshell fundamental parameters such as photoionization cross sections, FYs, and CK factors using a calibrated wavelength-dispersive grating spectrometer [39].

B. Line widths

The linewidth measurements were carried out at the Swiss Light Source (SLS) of the Paul Scherrer Institute (PSI), in Villigen, Switzerland, using the von Hamos Bragg-type bent crystal spectrometer of the University of Fribourg [40]. The spectrometer was installed at the beamline PHOENIX, downstream from the experimental chamber of end station I. The synchrotron radiation from the elliptical undulator was monochromatized with a Beryl(1-10) double-crystal monochromator. Upper harmonics were suppressed with dedicated mirrors. To probe the possible broadening of the $L\alpha_{1,2}$ and $L\beta_1$ lines of interest by partly overlapping M satellites originating from $L_{1,2}$-L_3M and L_1-L_2M CK transitions, respectively, the measurements were performed at 1.23 keV (i.e., between the Ge L_3 and L_2 edges), 1.3 keV (between the L_2 and L_1 edges), and 1.45 keV (above the L_1 edge). For each beam energy the bandwidth was about 0.5 eV. The beam spot on the sample was 0.5 mm wide and 2.6 mm high and the flux was $5 \times 10^{10} - 10^{11}$ photons/s. The sample consisted of a 0.6-mm-thick Ge crystal wafer.

The spectrometer was operated in the slitless geometry and the fluorescence from the sample was measured at grazing emission angles so that the contribution of the apparent source width to the energy resolution of the spectrometer was negligibly small. For the diffraction of the fluorescence x rays, an 80 mm high $\times 20$ mm wide $\times 100$ μm thick Beryl(1-10) crystal, bent cylindrically to a radius of 25.4 cm, was employed. The diffracted x rays were collected with a 26 mm long $\times 8$ mm high back-illuminated CCD x-ray camera having a spatial resolution of 20 μm.

For the energy calibration of the spectrometer, the $K\alpha$ transition of Mg was measured and the energy of 1253.688(11) eV reported in Ref. [32] was assigned to the fitted centroid position of the $K\alpha_1$ line. This transition as well as the $L\alpha_1$ line of Se ($E = 1379.10$ eV) was also used to determine the instrumental response. It was found that the instrumental response of the von Hamos spectrometer operated in the slitless geometry could be well reproduced by a Lorentzian profile. The energy-dependent width of the latter was determined by subtracting the natural widths of the two transitions from the total transition widths obtained from the fitting procedure. The natural widths of the Mg $K\alpha_1$ and Se $L\alpha_1$ x-ray lines were derived from the atomic level widths reported by Campbell

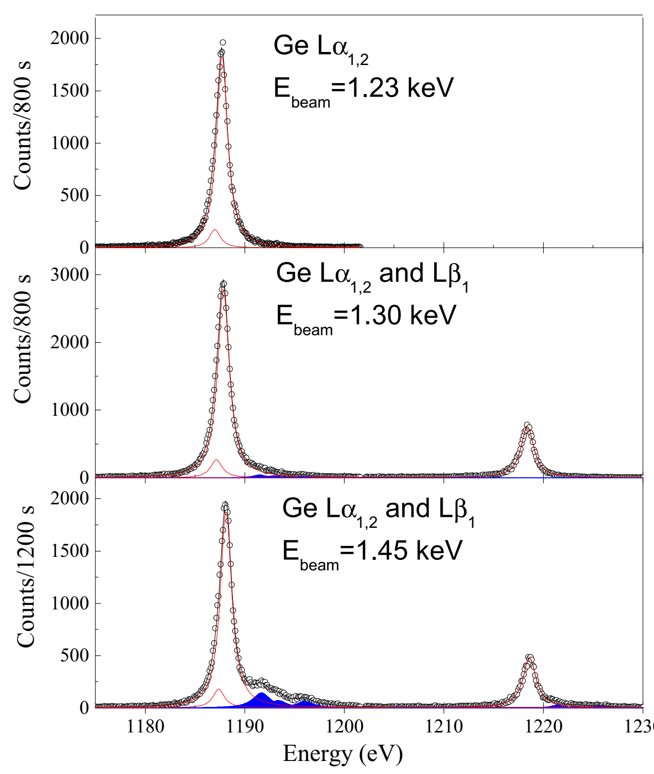

FIG. 4. (Color online) High-energy resolution $L\alpha_{1,2}$ (L_3-$M_{5,4}$ transition) and $L\beta_1$ (L_2-M_4 transition) x-ray spectra of a 0.6-mm-thick crystalline Ge wafer irradiated with monochromatic synchrotron radiation of different energies. Red curves correspond to the fits of the $L\alpha_2$ (weakest bump), $L\alpha_1$, and $L\beta_1$ diagram lines; filled (blue) areas, to M-shell satellites induced by CK transitions. In the fit the same width was assumed for the two components of the doublet, and the energy separation of the L_{α_2} and L_{α_1} lines was fixed at 0.75 eV according to the theoretical transition energies reported in Ref. [32]. The fit yields 0.13(1) for the intensity ratio of the L_{α_2}-to-L_{α_1} transitions.

and Papp [30]. Interpolating the so-obtained values for the energies corresponding to the $L\alpha_{1,2}$ and $L\beta_1$ transitions of Ge, instrumental FWHM broadenings of 0.63(3) and 0.61(3) eV, respectively, were found.

For illustration, the Ge L X-ray spectra measured at 1.23 keV (top), 1.30 keV (middle), and 1.45 keV (bottom) are depicted in Fig. 4. In the top panel the $L\beta_1$ line and the M satellites of the $L\alpha_{1,2}$ lines are not observed since the beam energy in this case was lower than the energy of the L_2 edge. In the middle panel (beam energy tuned between the L_2 and the L_1 edges), some weak satellite structure (relative intensity of 3.3%) due to L_2-L_3M CK transitions is visible for the $L\alpha_{1,2}$ transitions but not for the $L\beta_1$ one. In the bottom panel, which corresponds to a beam energy lying above the L_1 edge, a rich satellite structure (relative intensity of 21.3%) due mainly to L_1-L_3M CK transitions is observed for the $L\alpha_{1,2}$ lines, while some weaker M satellites (relative intensity of 9.4%), due to L_1-L_2M CK transitions, are also visible on the high-energy side of the $L\beta_1$ line. However, thanks to the high resolving power of the spectrometer, the M satellites could be well separated from their parent diagram lines and no significant broadening of the $L\alpha_{1,2}$ and $L\beta_1$ lines as a function of the beam energy was observed (see Table II).

IV. RESULTS AND DISCUSSION

A. Line widths and decay rates

In Table I we list the level widths for the L and M shells of Ge calculated in this work. They are compared to the corresponding EADL [31] atomic level widths and the values from Campbell and Papp [30]. The EADL database relies mostly on Dirac-Hartree-Slater calculations of Chen and Scofield. It is well known that this method seriously overpredicts the strength of CK transitions, resulting in erroneous fluorescent yields and widths. The database results are then normalized with the use of a Z dependence scaling for the FY, in which we encounter the familiar Z^4 dependence for the radiative yield. This approach is quite different from ours, as the calculations are performed with a Dirac-Fock approach, in which both radiative and nonradiative yields are obtained in the same frame set. Table II lists the theoretical line widths for the $L\alpha_1$ and $L\alpha_2$ lines and both the theoretical and the experimental linewidths for the $L_{\alpha_{1,2}}$ and L_{β_1} lines obtained in this work as well as the line widths of the two transitions derived from the EADL [31] atomic level widths and from the values recommended by Campbell and Papp [30]. As can be seen, there is a very good agreement between the calculated

TABLE III. Ge L-shell radiative decay rates for each value of the total angular momentum J_i of the initial configuration (in a.u.). The total value for each final configuration, and for each value of J_i, takes into account the statistical weight of each initial level i.

	$J_i = 1/2$	$J_i = 3/2$	$J_i = 5/2$	$J_i = 7/2$	Total	%
L_1-L_1	6.50×10^{-16}	7.48×10^{-17}	1.17×10^{-16}		8.42×10^{-16}	<0.001
L_1-L_2	1.12×10^{-05}	1.48×10^{-05}	1.76×10^{-05}		4.37×10^{-05}	0.436
L_1-L_3	2.97×10^{-05}	5.97×10^{-05}	5.98×10^{-05}		1.49×10^{-04}	1.486
L_1-M_1	3.22×10^{-07}	4.36×10^{-07}	5.02×10^{-07}		1.26×10^{-06}	0.013
L_1-M_2	6.64×10^{-04}	1.37×10^{-03}	1.33×10^{-03}		3.36×10^{-03}	33.445
L_1-M_3	1.21×10^{-03}	2.48×10^{-03}	2.53×10^{-03}		6.21×10^{-03}	61.851
L_1-M_4	3.13×10^{-06}	9.02×10^{-06}	3.88×10^{-06}		1.60×10^{-05}	0.160
L_1-M_5	4.81×10^{-06}	6.93×10^{-06}	1.22×10^{-05}		2.39×10^{-05}	0.238
L_1-N_1	7.47×10^{-08}	1.01×10^{-07}	1.12×10^{-07}		2.87×10^{-07}	0.003
L_1-N_2	6.37×10^{-05}	1.26×10^{-04}	4.85×10^{-05}		2.38×10^{-04}	2.369
Total	1.98×10^{-03}	4.06×10^{-03}	4.00×10^{-03}		1.00×10^{-02}	
L_2-L_2	1.78×10^{-15}	1.26×10^{-15}	1.66×10^{-16}		3.20×10^{-15}	<0.001
L_2-L_3	4.03×10^{-11}	8.32×10^{-11}	8.32×10^{-11}		2.07×10^{-10}	<0.001
L_2-M_1	1.37×10^{-04}	2.67×10^{-04}	2.60×10^{-04}		6.65×10^{-04}	4.250
L_2-M_2	3.64×10^{-07}	4.19×10^{-07}	5.82×10^{-07}		1.37×10^{-06}	0.009
L_2-M_3	5.14×10^{-07}	9.88×10^{-07}	8.79×10^{-07}		2.38×10^{-06}	0.015
L_2-M_4	2.38×10^{-03}	4.74×10^{-03}	4.38×10^{-03}		1.15×10^{-02}	73.507
L_2-M_5	5.74×10^{-04}	1.00×10^{-03}	1.27×10^{-03}		2.84×10^{-03}	18.171
L_2-N_1	5.21×10^{-04}	8.54×10^{-05}	1.59×10^{-05}		6.23×10^{-04}	3.982
L_2-N_2	8.19×10^{-06}	1.47×10^{-06}	1.74×10^{-08}		9.67×10^{-06}	0.062
Total	3.62×10^{-03}	6.09×10^{-03}	5.93×10^{-03}		1.56×10^{-02}	
L_3-L_3	1.19×10^{-16}	2.06×10^{-15}	1.54×10^{-16}	1.46×10^{-16}	2.48×10^{-15}	<0.001
L_3-M_1	1.43×10^{-04}	4.67×10^{-04}	4.16×10^{-04}	3.70×10^{-04}	1.40×10^{-03}	4.771
L_3-M_2	2.47×10^{-07}	8.59×10^{-07}	6.64×10^{-07}	7.87×10^{-07}	2.56×10^{-06}	0.009
L_3-M_3	3.14×10^{-07}	1.72×10^{-06}	1.43×10^{-06}	1.07×10^{-06}	4.53×10^{-06}	0.015
L_3-M_4	1.08×10^{-03}	1.94×10^{-03}	2.15×10^{-03}	2.44×10^{-04}	5.42×10^{-03}	18.517
L_3-M_5	1.71×10^{-03}	7.35×10^{-03}	6.11×10^{-03}	7.13×10^{-03}	2.23×10^{-02}	76.247
L_3-N_1	2.86×10^{-05}	5.16×10^{-05}	2.55×10^{-05}	2.29×10^{-05}	1.29×10^{-04}	0.439
L_3-N_2	5.23×10^{-07}	6.99×10^{-07}	1.48×10^{-08}	1.20×10^{-08}	1.25×10^{-06}	0.004
Total	2.96×10^{-03}	9.81×10^{-03}	8.71×10^{-03}	7.76×10^{-03}	2.92×10^{-02}	

TABLE IV. L-shell radiationless decay rates for Ge as a function of the initial-state total angular momentum J_i (in a.u.). L_1-L_2-$L_{2,3}M_{1\ldots5}N_{1,2}$ means that after the radiationless transition the atom with an initial L_1-subshell vacancy ends up with a vacancy in the L_2 subshell and another vacancy in either the $L_{2,3}$, the $M_{1\ldots5}$, or the $N_{1,2}$ shell. The total value for each final-state shell, and for each J_i, takes into account the statistical weight of each J_i.

	$J_i = 1/2$	$J_i = 3/2$	$J_i = 5/2$	$J_i = 7/2$	Total	%
L_1-L_2-$L_{2,3}M_{1\ldots5}N_{1,2}$	3.48×10^{-01}	7.13×10^{-01}	7.52×10^{-01}		$1.81 \times 10^{+00}$	27.003
L_1-L_3-$L_3M_{1\ldots5}N_{1,2}$	8.70×10^{-01}	$1.64 \times 10^{+00}$	$1.68 \times 10^{+00}$		$4.18 \times 10^{+00}$	62.271
L_1-M_1-$M_{1\ldots5}N_{1,2}$	8.98×10^{-02}	1.80×10^{-01}	1.80×10^{-01}		4.50×10^{-01}	6.704
L_1-M_2-$M_{2\ldots5}N_{1,2}$	1.68×10^{-02}	3.39×10^{-02}	3.47×10^{-02}		8.53×10^{-02}	1.271
L_1-M_3-$M_{3\ldots5}N_{1,2}$	2.45×10^{-03}	4.75×10^{-03}	4.07×10^{-03}		1.13×10^{-02}	0.168
L_1-M_4-$M_{4,5}N_{1,2}$	3.09×10^{-02}	6.19×10^{-02}	6.25×10^{-02}		1.55×10^{-01}	2.310
L_1-M_5-$M_5N_{1,2}$	3.70×10^{-03}	7.32×10^{-03}	6.83×10^{-03}		1.78×10^{-02}	0.266
L_1-N_1-$N_{1,2}$	8.39×10^{-05}	1.68×10^{-04}	1.82×10^{-04}		4.34×10^{-04}	0.006
L_1-N_2-N_2	1.67×10^{-07}	2.17×10^{-07}	4.01×10^{-07}		7.86×10^{-07}	<0.001
Total	$1.36\times10^{+00}$	$2.64\times10^{+00}$	$2.72\times10^{+00}$		$6.72\times10^{+00}$	
L_2-L_3-$L_3M_{1\ldots5}N_{1,2}$	2.48×10^{-03}	5.00×10^{-03}	4.92×10^{-03}		1.24×10^{-02}	1.216
L_2-M_1-$M_{1\ldots5}N_{1,2}$	1.56×10^{-02}	3.12×10^{-02}	3.07×10^{-02}		7.75×10^{-02}	7.599
L_2-M_2-$M_{2\ldots5}N_{1,2}$	8.79×10^{-02}	1.96×10^{-01}	1.95×10^{-01}		4.78×10^{-01}	46.916
L_2-M_3-$M_{3\ldots5}N_{1,2}$	2.19×10^{-02}	2.86×10^{-02}	2.89×10^{-02}		7.94×10^{-02}	7.789
L_2-M_4-$M_{4,5}N_{1,2}$	4.61×10^{-02}	1.20×10^{-01}	1.22×10^{-01}		2.88×10^{-01}	28.223
L_2-M_5-$M_5N_{1,2}$	2.81×10^{-02}	2.95×10^{-02}	2.65×10^{-02}		8.41×10^{-02}	8.248
L_2-N_1-$N_{1,2}$	1.87×10^{-05}	3.82×10^{-05}	5.38×10^{-06}		6.23×10^{-05}	0.006
L_2-N_2-N_2	9.92×10^{-06}	1.83×10^{-05}	1.40×10^{-06}		2.96×10^{-05}	0.003
Total	2.02×10^{-01}	4.10×10^{-01}	4.08×10^{-01}		$1.02 \times 10^{+00}$	
L_3-M_1-$M_{1\ldots5}N_{1,2}$	1.63×10^{-02}	5.36×10^{-02}	4.75×10^{-02}	4.21×10^{-02}	1.59×10^{-01}	7.508
L_3-M_2-$M_{2\ldots5}C_{1,2}$	6.45×10^{-02}	2.17×10^{-01}	1.83×10^{-01}	1.65×10^{-01}	6.29×10^{-01}	29.621
L_3-M_3-$M_{3\ldots5}N_{1,2}$	5.23×10^{-02}	1.72×10^{-01}	1.63×10^{-01}	1.40×10^{-01}	5.27×10^{-01}	24.806
L_3-M_4-$M_{4,5}N_{1,2}$	5.93×10^{-02}	2.05×10^{-01}	1.88×10^{-01}	1.67×10^{-01}	6.19×10^{-01}	29.137
L_3-M_5-$M_5N_{1,2}$	2.24×10^{-02}	6.52×10^{-02}	5.39×10^{-02}	4.80×10^{-02}	1.89×10^{-01}	8.918
L_3-N_1-$N_{1,2}$	3.97×10^{-05}	7.09×10^{-05}	9.41×10^{-06}	3.09×10^{-06}	1.23×10^{-04}	0.006
L_3-N_2-N_2	2.12×10^{-05}	3.24×10^{-05}	4.43×10^{-07}	2.93×10^{-06}	5.69×10^{-05}	0.003
Total	2.15×10^{-01}	7.13×10^{-01}	6.35×10^{-01}	5.62×10^{-01}	$2.12 \times 10^{+00}$	

and the measured values of the $L\beta_1$ line width, less than 2%, well inside the 1σ interval.

For the $L_{\alpha_{1,2}}$ line, however, we find a discrepancy of about 10% between the theoretical predictions and the experimental values. Note that because the $L_{\alpha_{1,2}}$ line is composed of a manifold of superimposed $L\alpha_1$ and $L\alpha_2$ transitions a direct comparison between the measured and the calculated $L\alpha_1$ and $L\alpha_2$ linewidths is not possible when only two Lorentzian functions are used to fit the experimental spectrum as shown in Fig. 4. Therefore, for a meaningful comparison, the FWHM of the experimental and synthesized $L_{\alpha_{1,2}}$ spectrum was considered. To extract the FWHM values for the $L_{\alpha_{1,2}}$ doublet the experimental spectra for the three beam energies were fitted with a single Lorentzian and an experimental broadening of 0.63 eV was subtracted. An average natural line width of 0.848(60) eV was found, which lies about 10% below the theoretical value listed in Table II.

Finally, as reported in Table II, a tiny change of the width with the beam energy is observed. The change is hardly significant in view of the quoted uncertainties (± 0.060 eV). Nevertheless, it seems that there is a trend for a slight increase in the width with increasing beam energy. This increase can be explained by unresolved N satellites resulting from N-shell shake processes following the creation by photoionization of the primary L_3 hole and also, for the highest beam energy, by L_1L_3N and L_2L_3N CK transitions, which lead to $L_3^{-1}N^{-1}$ double-vacancy states.

In Table III, we list the computed radiative decay rates (in a.u.) for Ge. The values listed represent the sums, for all final one-hole levels for each one-hole initial configuration, arranged by their initial total angular momentum, J_i. The statistical weight of each initial level is taken into account in the final results. These decay rates include the sum over all possible electric and magnetic multipoles. The first column identifies the initial and final one-hole configurations: For example, L_2-M_4 means that a hole from the L_2 subshell moves to the M_4 subshell, emitting a photon in the process. The final column presents the contribution of each final subshell to the total radiative decay rate of the initial subshell.

The theoretical radiationless transition probability values for the L shell of Ge are listed in Table IV. In this table, the values in each cell represent the sum over the final two-hole levels, for a fixed initial one-hole configuration with a given initial total angular momentum, J_i, and fixing one of the two resulting final holes. The values listed also include the statistical weight factor $(2J_i + 1)$. The notation used in the first column reflects these sums: for instance, the L_1-L_2-$L_{2,3}M_{1\ldots5}N_{1,2}$ line means that an initial configuration

TABLE V. L-subshell fluorescence yield values for Ge.

	ω_{L_1}	ω_{L_2}	ω_{L_3}
This work			
Theoretical	1.49×10^{-3}	1.51×10^{-2}	1.36×10^{-2}
Experimental			$1.20(11) \times 10^{-2}$
Puri *et al.* (RDHS) (1993) [41]	1.05×10^{-3}	1.42×10^{-2}	1.36×10^{-2}
McGuire (1971) [44]	7.70×10^{-4}		1.44×10^{-2}
Chen *et al.*(1971) [45]		7.72×10^{-3}	
Krause (1979) [43]	2.40×10^{-3}	1.30×10^{-2}	1.50×10^{-2}

with a hole in the L_1 subshell decays to a final state with one hole in the L_2 subshell and a second hole in either the $L_{2,3}$, the $M_{1\ldots5}$, or the $N_{1,2}$ subshell.

In the final column we list, as a percentage of the total, the contribution of each group to the total decay rates. We conclude that the contribution of the CK transitions in the L_1 one-hole initial configuration is about 89%, i.e., the computational effort to calculate the other contributions represent less than 11% of the total value. Regarding the initial configurations with one hole in the L_2 and L_3 subshells, the contributions are much more spread out through all the final two-hole levels.

B. Fluorescence yields

The theoretical FYs ω_{L_1}, ω_{L_2}, and ω_{L_3} were derived from Eq. (7) from the radiative and radiationless rates presented in the previous subsection. The obtained results ($\omega_{L_1} = 0.00149$, $\omega_{L_2} = 0.0151$, and $\omega_{L_3} = 0.0136$) are listed in Table V together with the experimental value of ω_{L_3} determined in this work and with the theoretical values obtained by other authors. Regarding the ω_{L_1}, ω_{L_2} FYs, they have not been determined experimentally yet. For the ω_{L_3} FY, a discrepancy of about 12% between the calculated and the measured value is found. However, comparing the results to those of other authors, we find a $<1\%$ difference with the RDHS value of Puri [41], recommended by Campbell [42] in his compilation, a 10% discrepancy with the result from Krause [43], and a 5% shift from the calculated value of McGuire [44]. On the other hand, the comparison with the theoretical results on the L_1 and L_2 subshells from the other authors raises some questions. For instance, the results of Chen *et al.* [45] and McGuire *et al.* [44] reveal a discrepancy of almost 50% with our results. Comparing with the results of Krause, we see a 61% deviation for the L_1 subshell and 14% for L_2.

V. CONCLUSIONS

In this work, we have presented the results of a collaboration between experimental and theoretical groups, within the International Initiative on X-Ray Fundamental Parameters framework, to obtain decay rates and FYs for Ge. The Dirac-Fock method, including relativistic and QED corrections, has been used to obtain the wave functions and binding energy values, as well as the L-shell radiative and radiationless decay rates, for Ge. This approach leads to FY values of 0.00149, 0.0151, and 0.136 for the L_1, L_2, and L_3 subshells, respectively. We have estimated the uncertainty of the FY to be 3%, by error propagation of Eq. (6). The individual uncertainty of the partial width $\Gamma^{R}_{S_n}$ was calculated as the average of the transition rate differences between the length and the velocity gauge, weighted by the transition rates themselves. Due to the impossibility of using the same procedure for Auger rates, but bearing in mind that the quality of the wave functions should be similar for two-hole states, we have adopted for the uncertainty of $\Gamma^{NR}_{S_n}$ the same value as the uncertainty of $\Gamma^{R}_{S_n}$. This led to final uncertainties of less than 3% in the FYs for the L_1, L_2, and L_3 subshells.

The experimental value of $\omega_{L_3} = 0.0120$, with an uncertainty of 9.2%, was determined at the PTB undulator beamline at the synchrotron radiation facility BESSY II in Berlin, employing calibrated instrumentation. The line widths of $L\alpha_{1,2}$ and L_{β_1} were measured at the SLS, PSI, Switzerland, using monochromatized synchrotron radiation and a von Hamos crystal spectrometer. The measured FYs and line widths were compared to the corresponding calculated values. We consider that this combined theoretical and experimental work on x-ray fundamental parameters has to be extended to other elements and shells in order to benchmark the theoretical methods employed here.

ACKNOWLEDGMENTS

J.H. and J.-Cl.D. would like to thank Dr. T. Huthwelker and the crew of the PSI/SLS beamline PHOENIX for the preparation of the synchrotron radiation beam employed for the line-width measurements. This research was supported in part by Fundação para a Ciência e a Tecnologia (FCT), Portugal, through Projects No. PEstOE/FIS/UI0303/2011 and No. PTDC/FIS/117606/2010, financed by the European Community Fund FEDER through COMPETE. We also thank the Allianz Program of the Helmholtz Association, Contract No. EMMI HA-216 (Extremes of Density and Temperature: Cosmic Matter in the Laboratory). M.G. and T.I.M. acknowledge the support of the FCT under Contracts No. SFRH/BPD/92455/2013 and No. SFRH/BPD/69627/2010, respectively. Laboratoire Kastler Brossel is Unité Mixte de Recherche du CNRS, de l' ENS et de l'UPMC No. 8552. The authors acknowledge financial support for the experimental determination of FP data by the REXDAB Collaboration that was initiated within the International Fundamental Parameter Initiative (www.exsa.hu).

[1] D. Coster and R. D. L. Kronig, Physica **2**, 13 (1935).
[2] R. Jenkins, R. Manne, R. Robin, and C. Senemaud, X Ray Spectrom. **20**, 149 (1991).
[3] G. H. Zschornack, *Handbook of X-Ray Data* (Springer, Berlin, 2007).
[4] R. W. Fink, R. C. Jopson, H. Mark, and C. D. Swift, Rev. Mod. Phys. **38**, 513 (1966).
[5] E. J. McGuire, Phys. Rev. A **2**, 273 (1970).
[6] D. L. Walters and C. P. Bhalla, Phys. Rev. A **3**, 1919 (1971).

[7] W. Bambynek, B. Crasemann, R. W. Fink, H. U. Freund, H. Mark, C. D. Swift, R. E. Price, and P. V. Rao, Rev. Mod. Phys. **44**, 716 (1972).
[8] C. P. Bhalla, J. Phys. B: At. Mol. Phys. **3**, 916 (1970).
[9] M. H. Chen, B. Crasemann, and H. Mark, Phys. Rev. A **21**, 436 (1980).
[10] M. H. Chen, B. Crasemann, and H. Mark, Phys. Rev. A **24**, 177 (1981).
[11] M. H. Chen, B. Crasemann, and H. Mark, Phys. Rev. A **21**, 449 (1980).
[12] M. H. Chen, B. Crasemann, and H. Mark, Phys. Rev. A **27**, 2989 (1983).
[13] J. M. Sampaio, T. I. Madeira, J. P. Marques, F. Parente, A. M. Costa, P. Indelicato, J. P. Santos, M. C. Lépy, and Y. Ménesguen, Phys. Rev. A **89**, 012512 (2014).
[14] J. M. Sampaio, F. Parente, P. Indelicato, and J. P. Marques, J. Phys. B: At. Mol. Opt. Phys. **46**, 065001 (2013).
[15] K. Kozio, J. Quant. Spectrosc. Radiat. Transfer **149**, 138 (2014).
[16] B. Beckhoff and G. Ulm, Adv. X-Ray Anal. **44**, 349 (2001).
[17] Y. Ménesguen and M. C. Lépy, Nucl. Instr. Methods B **268**, 2477 (2010).
[18] T. L. Hopman, C. M. Heirwegh, J. L. Campbell, M. Krumrey, and F. Scholze, X Ray Spectrom. **41**, 164 (2012).
[19] B. Beckhoff, J. Anal. At. Spectrom. **23**, 845 (2008).
[20] J. P. Desclaux, Comput. Phys. Commun. **9**, 31 (1975).
[21] P. Indelicato and J. Desclaux, *Mcdfgme, a Multiconfiguration Dirac-Fock and General Matrix Elements Program* (2005), http://kroll.lkb.upmc.fr/mcdf/.
[22] P. Indelicato, O. Gorveix, and J. P. Desclaux, J. Phys. B: At. Mol. Phys. **20**, 651 (1987).
[23] O. Gorceix, P. Indelicato, and J. P. Desclaux, J. Phys. B: At. Mol. Phys. **20**, 639 (1987).
[24] P. Indelicato, Nucl. Instr. Methods B **31**, 14 (1988).
[25] J. P. Santos, J. P. Marques, F. Parente, E. Lindroth, P. Indelicato, and J. P. Desclaux, J. Phys. B: At. Mol. Opt. Phys. **32**, 2089 (1999).
[26] P. Indelicato and J. P. Desclaux, Phys. Rev. A **42**, 5139 (1990).
[27] P. Indelicato, Phys. Rev. A **51**, 1132 (1995).
[28] P. Indelicato, Phys. Rev. Lett. **77**, 3323 (1996).
[29] P.-O. Löwdin, Phys. Rev. **97**, 1474 (1955).
[30] J. L. Campbell and T. Papp, At. Data Nucl. Data Tables **77**, 1 (2001).
[31] S. T. Perkins, D. E. Cullen, M.-H. Chen, J. H. Hubbell, J. Rathkopf, and J. H. Scofield, Lawrence Livermore National Laboratory Report UCRL-50400, **30** (1991).
[32] R. D. Deslattes, E. G. Kessler, P. Indelicato, L. de Billy, E. Lindroth, and J. Anton, Rev. Mod. Phys. **75**, 35 (2003).
[33] M. Mueller, B. Beckhoff, G. Ulm, and B. Kanngießer, Phys. Rev. A **74**, 012702 (2006).
[34] P. Hönicke, M. Kolbe, M. Müller, M. Mantler, M. Krämer, and B. Beckhoff, Phys. Rev. Lett. **113**, 163001 (2014).
[35] M. Kolbe, P. Hönicke, M. Müller, and B. Beckhoff, Phys. Rev. A **86**, 042512 (2012).
[36] B. Beckhoff, A. Gottwald, R. Klein, M. Krumrey, R. Muller, M. Richter, F. Scholze, R. Thornagel, and G. Ulm, Phys. Status Solidi B **246**, 1415 (2009).
[37] A. Gottwald, U. Kroth, M. Krumrey, M. Richter, F. Scholze, and G. Ulm, Metrologia **43**, S125 (2006).
[38] F. Scholze and M. Procop, X Ray Spectrom. **30**, 69 (2001).
[39] M. Muller, B. Beckhoff, R. Fliegauf, and B. Kanngiesser, Phys. Rev. A **79**, 032503 (2009).
[40] J. Hoszowska, J.-C. Dousse, J. Kern, and C. Rhme, Nucl. Instr. Methods Phys. Res. Sec. A: Accelerat. Spectrom. Detect. Assoc. Equip. **376**, 129 (1996).
[41] S. Puri, D. Mehta, B. Chand, N. Singh, and P. N. Trehan, X Ray Spectrom. **22**, 358 (1993).
[42] J. L. Campbell, At. Data Nucl. Data Tables **85**, 291 (2003).
[43] M. O. Krause, J. Phys. Chem. Ref. Data **8**, 307 (1979).
[44] E. J. McGuire, Phys. Rev. A **3**, 587 (1971).
[45] M. H. Chen, B. Crasemann, and V. O. Kostroun, Phys. Rev. A **4**, 1 (1971).